2019-01-01

Magnetic Nanoparticles For Hyperthermia For Cancer Treatment

Bianca Paola Meneses Brassea
University of Texas at El Paso

MAGNETIC NANOPARTICLES FOR HYPERTHERMIA FOR CANCER TREATMENT

BIANCA PAOLA MENESES BRASSEA

Master's Program in Physics

APPROVED:

Ahmed A. El-Gendy, Ph.D., Chair

Chunqiang Li, Ph.D.

Mahesh Narayan, Ph.D.

Stephen L. Crites, Jr., Ph.D.
Dean of the Graduate School

Dedication

I dedicate this thesis to my beloved family, my father Heriberto, my mother Lietta, my sister Alexia, and my brother Heriberto. They have supported me since I first began my Physics studies back at home and motivated me with love and patience to keep on studying and working hard to pursue my dreams.

“Did you ever know that you're my hero

And everything I would like to be?

I can fly higher than an eagle

For you are the wind beneath my wings”

MAGNETIC NANOPARTICLES FOR HYPERTHERMIA FOR CANCER TREATMENT

by

BIANCA PAOLA MENESES BRASSEA

THESIS

Presented to the Faculty of the Graduate School of

The University of Texas at El Paso

in Partial Fulfillment

of the Requirements

for the Degree of

MASTER OF SCIENCE

Department of Physics

THE UNIVERSITY OF TEXAS AT EL PASO

December 2019

Acknowledgements

First of all, I would like to thank Dr. Ahmed A. El-Gendy for letting me be part of his research group and his dream Nanoland Lab. He has been a great mentor who has taught me a lot about the beauty of nanomagnetics and biomaterials and has inspired me to continue in this research field. He is a true example of passion, dedication, and hard work.

The startup and rising stars funds by UTEP and UT-system respectively. Also, the research reported in this paper was partially supported by the National Institute of General Medical Sciences of the National Institutes of Health under linked award numbers RL5GM118969, TL4GM118971, and UL1GM118970.

I want to thank everyone in our Nanoland Lab team, especially MS Eduardo Martinez who helped me not only in the lab but also throughout our courses during our Master's.

Special thanks to the faculty and staff at the Physics Department for welcoming me as an international student, as well as my fellow classmates who I can also now call my friends. It is very nice to be part of such beautiful and supportive community. Dr. Jorge Lopez for inviting me to coming to Utep and helping me throughout my admission process.

The First Baptist Church's International Student Fellowship for all the support their members have given me since I arrive to El Paso in Spring 2018. They became my family and for that I will always be grateful. God bless.

My dear and beloved friends back at home for being my mental and emotional strength throughout my graduate studies. Their friendship, love, support, and motivation kept me from ever giving up.

And last but not least, my dear family. I wouldn't be here if it weren't for them. Their love is the force that keeps me moving forward. I love you. Thank you so much for your love

and constant support, for your words of encouragement, and for believing in me no matter how many obstacles I've encountered on my way. For reminding me that I am invincible, unbreakable, unstoppable, unshakable, and that if I get knocked down, I will get up again. Thank you. I love you such. God bless

Table of contents

List of tables

List of figures

Chapter 1: Introduction

Since the beginning of this century, nanotechnology has become a very relevant research field due to its ability to provide many resources for different applications such as environmental, industrial, and medical [1-3]. The study of magnetic nanoparticles for medical applications, such as diagnosis, tissue repair, drug delivery, magnetic resonance imaging (MRI), and magnetic hyperthermia for cancer treatment [3-8], has become an important research field in the scientific community due to the properties the magnetic particles present at nanometric scale.

In this thesis I will focus on the synthesis, characterization, and feasibility for cancer treatment through magnetic hyperthermia of two different materials: Fe_3O_4 (magnetite) and Ni_xCu_{4-x}. The study of Fe_3O_4 (magnetite) nanoparticles has become important since they are the type of iron oxide that presents the best magnetic properties, size, morphology, feasibility, nontoxicity, and dispersion enhancement through surface functionalization [9, 10]. The superparamagnetic behavior of the magnetic nanoparticles has become of great relevance since they can be easily manipulated by the application of an alternate current magnetic field (ACMF). On the other hand, the relevance of the study of Ni_xCu_{4-x} reflects on the use of a ferromagnetic material for self-regulating magnetic hyperthermia treatment (SRMH)[11].

Super paramagnetic-like iron oxide nanoparticles have been used for medical applications for more than 20 years [12]. One of the biggest challenges that has been encountered is that the iron oxide nanoparticles agglomerate because they are highly magnetic, making it very difficult to get good dispersion in solutions, such as water. On the other hand, it is possible to obtain particles of small size with very good nanometric distribution. Most of the materials have

toxicity at nanoscale, which is why we chose to study iron oxide nanoparticles, specifically Fe_3O_4 (magnetite), because they present nontoxicity and have FDA approval for MRI [12].

Ni_xCu_{4-x} alloys are ferromagnetic materials. The reason why we study them for magnetic hyperthermia treatment is due to their Curie temperature (T_c). When an ACMF is applied and Tc is achieved, the heating reaches saturation, which allows a controlled and safe application of magnetic hyperthermia treatment. This will further be explained in more detail.

1.1 Nanotechnology

Nanotechnology refers to the methods and techniques required for the study, design, and fabrication of new materials at a nanometric scale. 1 nanometer (nm) is the millionth part of a millimeter (mm), this is $1x10^{-9}$ m. Figure 1[13] shows an example nanoscale to have a clearer idea of the size of nanoparticles.

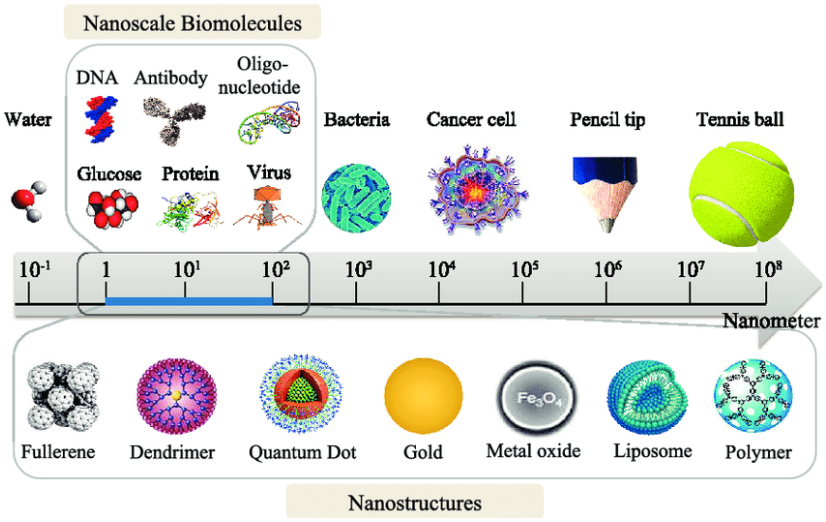

Figure 1 Nanoscale

The development of nanomaterials provides a vast versatility in design and preparation methods since they possess a great variety of chemical, physical, and functional properties, which allow the enhancement of people's daily life.

Nanomaterials have been obtained and utilized along human history. They can be found in the stained glass windows of churches as gold nanoparticles, war instruments as nanotubes, or decorations such as the famous cup of Lycurgus[14], which is 1600 years old. After the conference given by Richard P. Feymann (Physics Nobel) at the American Physical Society in 1959, titled "*There's a plenty room at the bottom*", research on new nanomaterials began[14]. In 1988, Harold Kroto, Robert Curl, and Richard Smalley discovered fullerenes and in 1991, carbon nanotubes were discovered by Sumio Iijima [15]. These advances allowed a better understanding on the research of experimental techniques of synthesis and characterizacion of nanomaterials, as well as the applications they have in all the science and engineering fields.

Nanoparticles (NPs) are ultrafine particles with at least one dimension in the nanoscale (1 to 500 nm). They are extremely versatile, reactive and strong compared to bulk. They can be classified into 2 different groups: organic, like carbon nanotubes, liposomes, and fullerenes; and inorganic, like quantum dots, metallic, and magnetic nanoparticles (MNPs) [16-18]. Magnetic nanoparticles have become very popular due to their ability to be easily manipulated by applying an alternate current magnetic field (ACMF) and utilized in different applications.

It is of great importance to provide a detailed description of the main magnetic properties and behaviors that nanoparticles possess to understand the different ways they can be taken advantage of.

1.2 Magnetic behavior

Magnetism is a property of matter that happens as a consequence of the existence of particles with mass and charge (for example, electrons), that when they spin, they create a magnetic dipole [19]. It is a distribution of atomic magnetic moments, whose contribution to the total magnetic moment of a given material can be described, from a macroscopic point of view, as a volumetric density of magnetic moment. This is called magnetization M and is given by $M = \frac{dM}{dV}$ [A/m], which can also be expressed in terms of a vector quantity called magnetic polarization J given by $J = \mu_0 \frac{dM}{dV} = \mu_0 M$ [T= V·s/m^2], where μ_0 is the magnetic field constant which has a value of $4\pi \cdot 10^{-7}$ [V·s/A·m]. Both magnitudes, M and J, determine to some extent the degree of alignment of the elemental magnetic moments in the material.

1.2.1 Magnetic induction

When a magnetic field **H** is applied to a material, this can be either attracted by the strong region of the field or repelled by it. This means that a magnetic field **B**, called magnetic induction, is induced in the material and it interacts with the external field **H**. In a general case, in which we consider all the possible sources of **B** (currents, magnetized matter, …), the relation between the magnetic induction **B** and the intensity of the magnetic field **H** is given by the next equation:

$$\boldsymbol{B} = \mu_0(H + M) = \mu_0 H + J \qquad [\text{T}=\text{V}\cdot\text{s/m}^2] \qquad (1)$$

This is one of the most important relations in the magnetism of materials. In vacuum, **M** and **J** are equal to zero and equation (1) becomes

$$\mathbf{B} = \mu_0 \mathbf{H}. \qquad (2)$$

M and **J** are proportional to the magnetic field **H**.

Now, in the case of isotropic materials, in which **M** and **J** collinear (parallel to **H**), the next expressions can be written:

$$\boldsymbol{M} = \chi \boldsymbol{H} \;\rightarrow\; \chi = \frac{\boldsymbol{M}}{\boldsymbol{H}} \qquad \text{(no dimensions)} \tag{3}$$

$$\boldsymbol{J} = \chi \boldsymbol{H} \;\rightarrow\; \chi = \frac{\boldsymbol{J}}{\boldsymbol{H}} \qquad \text{(Henry/m= V·s/A·m)} \tag{4}$$

where χ is a characteristic parameter of the material, called magnetic susceptibility, which can be defined as the relation between the magnetic polarization of the material and the magnetic field at which it is exposed. The magnetic susceptibility of a material can be described as its feasibility to be magnetized by a given magnetic field **H**. If we now substitute equation (3) in equation (1), we get the next expression:

$$\boldsymbol{B} = \mu_0(\boldsymbol{H} + \boldsymbol{M}) = \mu_0(1 + \chi)\mathbf{H} \quad \rightarrow \quad \mathbf{B} = \mu \boldsymbol{H} \qquad [\text{T}] \tag{5}$$

where $\mu = \mu_0(1 + \chi)$ is the absolute magnetic permeability (no dimensions).

1.2.2 Classification of magnetic materials

Magnetic materials can be classified depending on the value of their magnetic susceptibility $\left(\chi = \frac{\boldsymbol{M}}{\boldsymbol{H}}\right)$. The different types of magnetic behavior are diamagnetism, paramagnetism, ferromagnetism, anti-ferromagnetism, ferrimagnetism, and superparamagnetism. The general ideas of these behaviors and the mechanisms of the phenomena the materials present will be discussed next, based on the fact that their magnetic properties depend on their electronic structure and the orbital movement of the electrons and their spin.

Diamagnetic materials

The diamagnetic materials are those whose atoms present complete atomic orbitals. Their magnetic moments are paired and the spin of their spins compensates, which makes the atoms magnetically neutral. The magnetic susceptibility (property that measures the degree of magnetization when exposed to an applied external magnetic field) of these materials is slightly negative, $\chi < 0$, and a magnetic field applied to them will be repelled[20]. This means, the magnetic moments align in the opposite direction of the applied magnetic field. Once the applied magnetic field is removed, the material goes back to its neutral state. In other words, under an applied external magnetic field **H**, the material is induced to a change in the orbital movement of its electrons so the magnetic moments, associated to the induced currents, produce a very small ($\neq 0$) magnetization. This magnetization **M** is opposite to the magnetic field **H** that causes it (Figure 2.b), resulting in a negative susceptibility χ. When $\mathbf{H}=0 \rightarrow \mathbf{M}=0$ and when $\mathbf{H} \neq 0 \rightarrow \mathbf{M} \neq 0$, which translates in a linear behavior between these two magnitudes. Diamagnetic behavior is not generally dependent on temperature.

Paramagnetic Materials

In paramagnetic materials, the spins align to the direction of the applied magnetic field because they orient towards the lowest energy state ($\chi > 0$, $\chi << 1$), resulting in magnetization $\mathbf{M} \neq 0$. When the magnetic field is removed, the spins randomly reorient and there is no remnant magnetic behavior left. This is, when $\mathbf{H} = 0$, the magnetic moments of the atoms and the spin of the uncoupled electrons have a random orientation, which results in $\mathbf{M} = 0$. The susceptibility of paramagnetic materials depends on the temperature (T). At room temperature T and low intensity magnetic field H, the magnetization or polarization of the material is relatively low, since there is a

thermal oscillation effect in its atomic structure that prevents a complete alignment of the magnetic moments. On the other hand, at low temperatures, this effect is reduced, enhancing the alignment of the magnetic moments to the applied magnetic field, hence resulting in higher magnetization[21, 22].

Ferromagnetic, ferrimagnetic, and antiferromagnetic materials

Ferromagnetic materials exhibit a strong magnetic behavior when submitted to an applied magnetic field and stay magnetized once the field is removed. This is due to their crystalline structure that allows a strong interaction between the magnetic moments. Ferromagnetic materials present a positive susceptibility, 10^3~10^{11} times higher than any of the other materials (χ>>1). Some examples of ferromagnetic materials are iron (Fe), cobalt (Co), and nickel (Ni), as well as alloys of these materials with other elements[23], and are considered the precursors of all magnetic materials and their applications. Ferromagnetic materials have a very wide range of temperature at which this behavior can be present, but once they reach Curie temperature (T_C, temperature above which certain materials lose their permanent magnetic properties), they become paramagnetic[24].

Ferrimagnetic materials are the ones in which some of the magnetic moments align with the direction of the applied magnetic field and some others align in the opposite direction, however, they have different magnitudes, which results in non-zero magnetization. Antiferromagnetic materials present a magnetic behavior in which some of the magnetic moments align with the direction of the applied magnetic field and some others in the opposite direction in a regular pattern. Antiferromagnetism exists at sufficiently low temperatures, but vanishes at and above Néel temperature (T_N), where the material becomes paramagnetic (analogous to Curie temperature)[25, 26].

These kinds of materials present a cooperative magnetic behavior with the purpose of decreasing the magnetostatic energy, which is the potential energy produced by the external magnetic field[27]. This behavior yields to the atomic spins having a parallel alignment in "sections" called magnetic domains, which are separated by regions called Bloch walls. Inside each domain, the spins are parallelly aligned, but their direction is different in each domain in a way that all of them compensate, resulting in zero magnetization. They are randomly oriented[28, 29]. a domain which is too big is unstable, and will divide into smaller domains. But a small enough domain will be stable and will not split, and this determines the size of the domains created in a material. This size depends on the balance of several energies within the material.[3] Each time a region of magnetization splits into two domains, it creates a domain wall between the domains, where magnetic dipoles (molecules) with magnetization pointing in different directions are adjacent. The exchange interaction which creates the magnetization is a force which tends to align nearby dipoles so they point in the same direction. Forcing adjacent dipoles to point in different directions requires energy. Therefore, a domain wall requires extra energy, called the domain wall energy, which is proportional to the area of the wall. Thus the net amount that the energy is reduced when a domain splits is equal to the difference between the magnetic field energy saved, and the additional energy required to create the domain wall. The field energy is proportional to the cube of the domain size, while the domain wall energy is proportional to the square of the domain size so, as the domains get smaller, the net energy saved by splitting decreases. The domains keep dividing into smaller domains until the energy cost of creating an additional domain wall is just equal to the field energy saved. Then the domains of this size are stable. In most materials the domains are microscopic in size, around 10^{-4} - 10^{-6} m[30]. Paramagnetic and diamagnetic materials, in which the dipoles align in response to an

external field but do not spontaneously align, do not have magnetic domains. When the size of a ferro or ferromagnetic material is reduced to the point where it reaches a critical size smaller than a domain, a single domain system is generated. This change is fundamental since it yields a new magnetic behavior: superparamagnetism[31].

Superparamagnetic materials

The superparamagnetic behavior is defined by having a high magnetic susceptibility, typical of ferro and ferrimagnetic materials, but with the characteristic of being able to turn the spins randomly under the influence of temperature (Curie temperature, T_C), characteristic of paramagnetism. This characteristic temperature is named after the French physicist Pierre Curie, who discovered it in 1895, who established that the magnetic susceptibility of paramagnetic substances depends on the inverse of the temperature, that is, that the magnetic properties change depending on the temperature. He found that in all ferromagnets there is a decrease in magnetization until the temperature reaches a critical value, where the magnetization becomes equal to zero; above the Curie temperature, ferromagnets behave like paramagnetic materials. The Curie temperature of magnetite (Fe_3O_4) is 858 K[32].

Superparamagnetic nanoparticles have zero coercivity (H_C), this is, the necessary magnetic field that would have to be applied to the particles to achieve demagnetization once the saturation magnetization Ms (state in which all domains of the material are oriented in the same direction) has been reached, is zero. Once the applied magnetic field is removed, they do not show any magnetization. This fact is fundamental, since it implies that the nanoparticles will not have magnetic activity until a magnetic field is applied and that the activity will be eliminated when the applied magnetic field is removed[33].

Figure 2 shows the magnetic behavior dependence on susceptibility χ with change in temperature T, whilst Figure 3 depicts the magnetization M versus an applied magnetic field H.

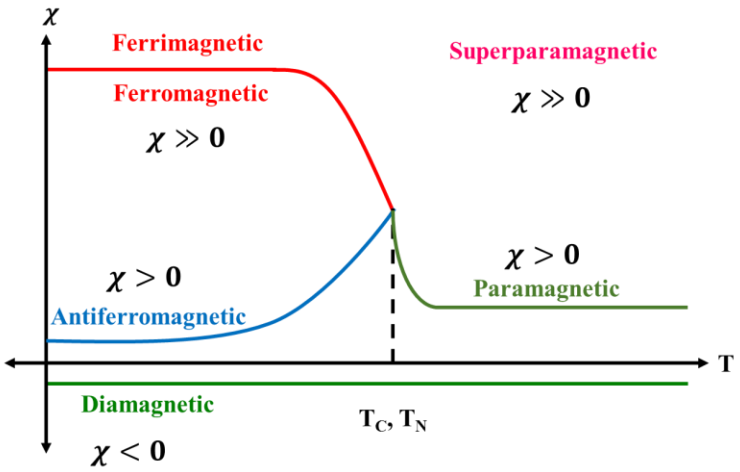

Figure 2 Susceptibility vs Temperature of magnetic materials

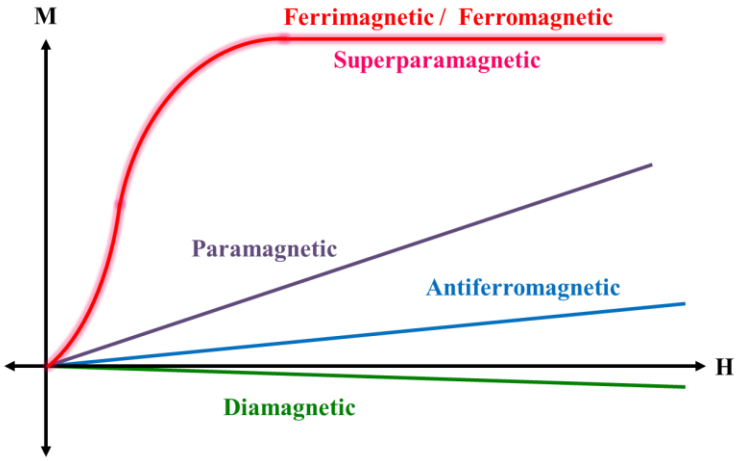

Figure 3 Magnetization vs Magnetic field

The hysteresis loop tells the history of magnetization and demagnetization of a ferromagnetic material when submitted to an applied magnetic field, as shown in Figure 4.

a) It starts with M=0. M increases as H increases. This curve is known as first saturation curve.

b) Once it reaches saturation magnetization Ms, M decreases as H decreases. The material starts to demagnetize, following a different path than in the first curve.

c) As it can be observed, when H=0, M≠0. This means the material stayed magnetized. If we now apply -H, the magnetic domains will orient in the opposite direction, decreasing the magnetization of the material.

d) As –H increases, –M increases until it reaches a saturation point, just like in the first curve but in the opposite direction.

e) Now H starts to increase, going from –H to H=0. –M decreases.

f) When –H reaches zero, the material preserves an induced magnetization. If we now apply H, the magnetic domains align in the opposite direction, decreasing the material's magnetization. As H increases, -M increases until it reaches zero.

g) If H continues increasing, the material will get magnetized until the alignment of the magnetic moments reaches its maximum. This means that, once again, we reach saturation magnetization Ms.

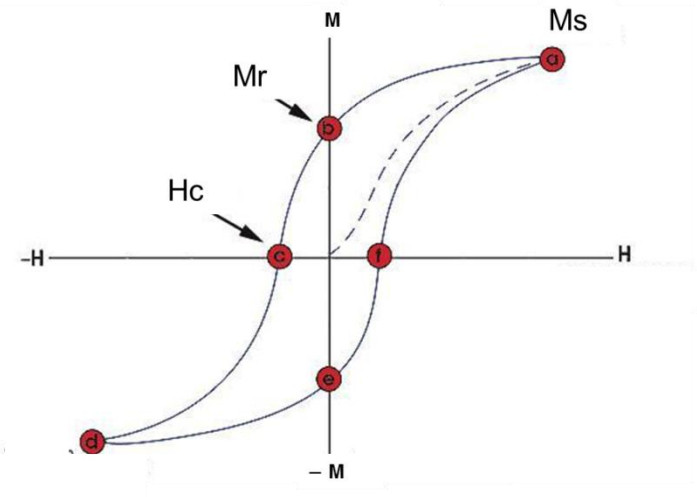

Figure 4 Hysteresis loop

The hysteresis loop of a ferromagnetic material can be "narrow" or "wide" depending on the composition of the material. Materials with a narrow hysteresis loop are called soft ferromagnetic materials and those with a wide hysteresis loop are called hard ferromagnets. Soft materials have a low coercive force. This means that the magnetization of the material can reverse its direction without dissipating much energy (loss of hysteresis). On the other hand, hard materials have a very high coercive force, which means that they are very resistant to demagnetizing, as in the case of permanent magnets[34, 35]. Figure 5 shows the hysteresis loops of soft and hard ferromagnetic materials.

In Figure 6 we can appreciate the hysteresis loops of the magnetic behaviors we have discussed so far.

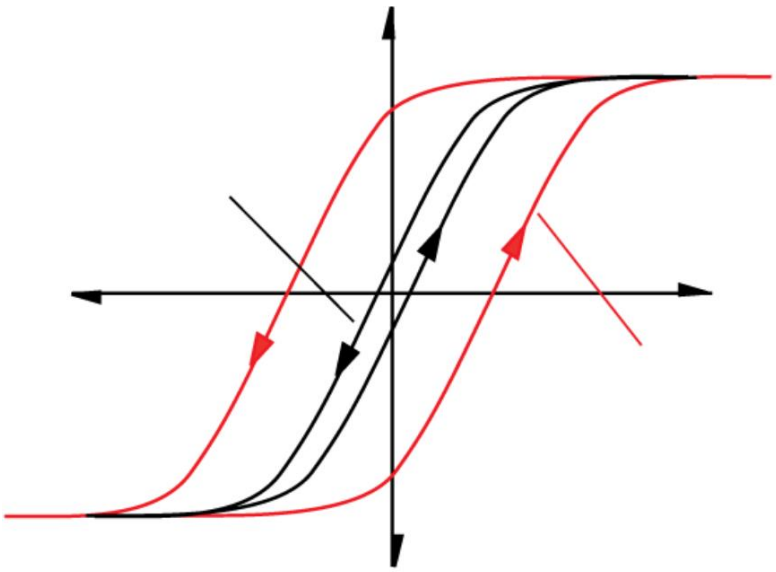

Figure 5 Hysteresis loops of soft and hard ferromagnetic materials[36]

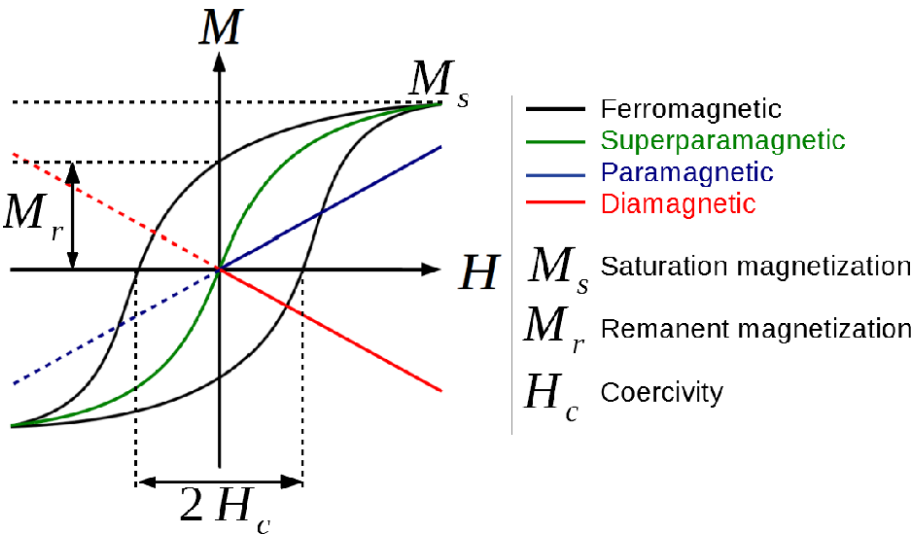

Figure 6 Hysteresis loops of the different magnetic behaviors[37]

1.3 Applications of magnetic nanoparticles

It is known that when a material is brought from bulk to nanoscale, its chemical and physical properties change. This yielded to the possibility of the use and study of nanomaterials in many research fields. The use and applications of magnetic nanoparticles depend on several parameters such as the precursors, the size distribution, the shape, the synthesis method, the interaction between particles, toxicity, biocompatibility, etc. Some of the most important applications of magnetic nanoparticles are environmental, industrial, and biomedical [38-46]. The preparation of ferrofluids using magnetic nanoparticles has been of high relevance in biomedical applications such as drug delivery, magnetic resonance imaging (MRI) as contrast agents, and magnetic hyperthermia treatment for cancer[47-58].

1.3.1 Magnetic hyperthermia for cancer treatment

Hyperthermia is commonly defined as an abnormal elevation of body temperature carried out artificially by means of external medical devices. Hyperthermia is typically used to mitigate or decrease cysts, inflammation, and pain caused by arthritis by increasing blood flow to provide

nutrition to the affected tissues and reduce muscle spasms. In addition, hyperthermia is applied in cancer treatment because cancer cells are significantly vulnerable to high temperatures compared to healthy cells. The sensitivity of cancer cells to high temperatures or heat is derived from insufficient oxygen in their own cells due to poor blood flow in the affected region. Healthy cells can systematically organize the blood flow in a remarkable way and dissipate any additional heat in the surrounding vascular system through conduction and convection. However, cancer cells show a lower capacity to promote a vascular system and, therefore, blood flow decreases and overheats (at a temperature above 42 ° C). Thus, the viability of the tumor cell is greatly reduced in the range of 41 ° C to 47 ° C, while healthy cells are hardly affected[57, 59]. Figure 7 shows the schematic diagram of magnetic hyperthermia treatment. First, a well dispersed solution of water and the magnetic nanoparticles is prepared. The ferrofluid is then injected into the cancerous tumor. Next, the patient is submitted to an ACMF, causing a rapid switching of the particles' magnetic moments, resulting in dissipated heat which kills the cancerous cells[60-64]. Dissipation is due to rotation of the entire magnetic particle within the surrounding liquid (Brownian relaxation) and/or the rotation of the magnetic moment within the magnetic core (Néel relaxation), as shown in Figure 8. Generally, heating power is dominated by the faster regime of relaxation[65].

Magnetic hyperthermia treatment for cancer has been the focus of many studies nowadays due its ability to provide a much less invasive and nonaggressive option for cancer treatment compared to other methods such as chemotherapy and radiotherapy. For magnetic hyperthermia, the ferrofluid is injected into the patient's tumor only once and the treatment requires only a few sessions of application of the ACMF. After that, the body discards the nanoparticles naturally. This is why it is important for the nanoparticles to present a

superparamagnetic-like behavior; they should only present magnetization in the presence of an ACMF and go back to being demagnetized once it is removed.

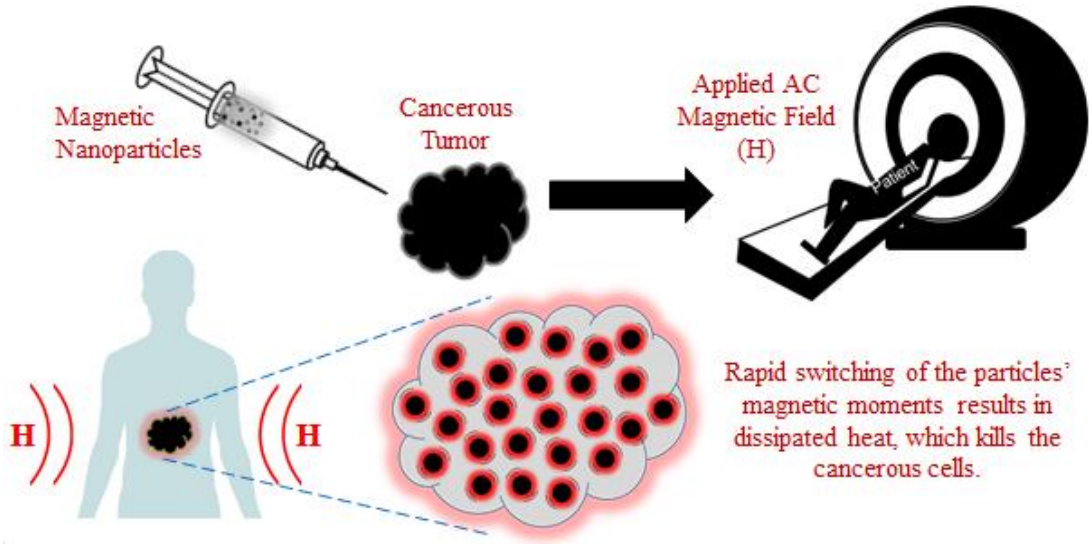

Figure 7 Schematic diagram of magnetic hyperthermia treatment

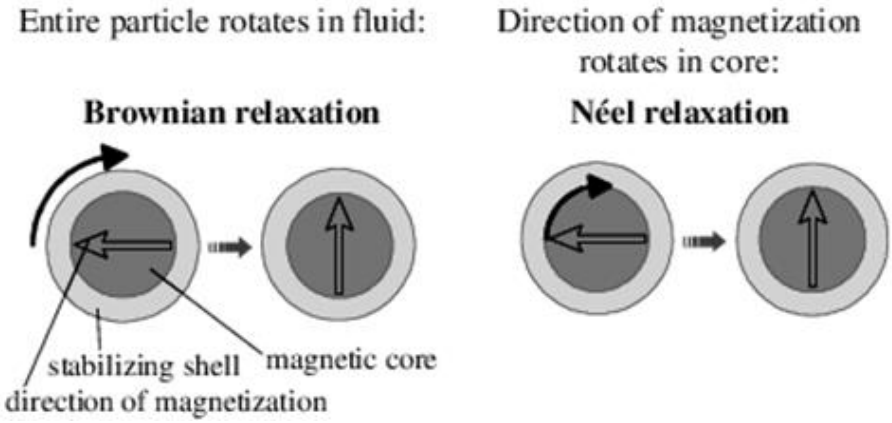

Figure 8 Néel and Brownian relaxation[66]

For the work at hand, two different samples of magnetic nanoparticles, Fe_3O_4 and Ni_xCu_{4-x}, were prepared and we will now move forward to describe the experimental details followed by

the presentation and discussion of the results obtained after characterization and measurements for hyperthermia.

Chapter 2: Experimental details

2.1 Synthesis methods

2.1.1 Synthesis of Fe_3O_4 nanoparticles

The synthesis of the Fe_3O_4 nanoparticles was carried out using 200 mg of iron (II) chloride tetrahydrate (99.99% from Fischer Scientific) and 200 mL of ethanol (190 proof from Fischer Scientific). The iron precursor and ethanol were placed into a sealed stainless-steel vessel (Parr & Instruments 4838) with argon. The vessel has been heated up to 275 °C where the pressure raised to 1650 psi (114 bar) for 2 hours. Then it was cooled down to room temperature where the sample was washed and collected. Synthesis was repeated for 320 °C and 350 °C, with pressure reaching 109 and 50 bar, respectively. For 350 °C, the temperature in the pressure reactor was reaching 138, which is not safe for the equipment, so we vented the vessel to release some pressure.

2.1.2 Synthesis of Ni_xCu_{4-x} nanoparticles

All the materials used in this work were highly pure and bought from Fisher Scientific: Cetyl trimethyl ammonium bromide (CTAB) which applied as pore directing agent, nickel (II) acetate tetrahydrate as nickel precursor, copper (I) chloride as copper precursor, sodium citrate, sodium borhydride as reducing agent, pure ethanol, and sodium hydroxide as precipitant in addition to hydrazine. The nickel-copper nanocomposite sample was prepared via wet chemistry. Nickel acetate powder and copper chloride powder were mixed in the desired composition (71 wt% nickel, 29 wt% copper). In order to obtain a highly distributed composition over the resulting nanocomposites, the mixture was stirred for 30 minutes, before it was fixed into crucible. The

product was collected and annealed up at 300 °C under vacuum condition for 1, 2, 3, 6, and 10 hours.

2.2 Characterization methods

2.2.1 Characterization of Fe_3O_4 nanoparticles

Crystal structure characterization of the sample was performed using Panalytical X-ray diffractometer with Cu K_α with radiation (λ = 1.5405 Å). The crystallite size of the nanoparticles was estimated from the peaks broadening using Scherer formula. Particles size and morphology of the sample were characterized using scanning-electron microscopy (Hitachi Regulus SEM). The magnetic properties of the sample were measured using the vibrating sample magnetometer VersaLab 3 Tesla (VSM) from quantum design. Hysteresis loop, MxH, was measured at 300 K, with DC magnetic fields up to H=3T. Zero-field-cooling/field-cooling (ZFC/FC) MxT curve was measured from 50 to 400 K. Finally, AC magnetic hyperthermia measurements were carried out using G2-D5 Series Multi-mode 1500W Driver from Nanoscale Biomagnetics. The Fe_3O_4 nanoparticles were dispersed in 1 mL of distilled water and placed into the equipment coil and the heat was detected by fiber optic sensor immersed in the particles solution. The concentration of the solution was 5.6 mg/mL.

2.2.2 Characterization of Ni_xCu_{4-x} nanoparticles

X-ray diffractometer by PANalytical Empyrean 2 revealed a cubic structure of the samples. FESEM JEOL640 scanning electron microscope and HRTEM JEOL-JEM-1230 transmission electron microscope were used to study the morphology of the nanoparticles. The magnetic properties were studied through vibrating sample magnetometry using Quantum Design VSM 3T Versalab instrument. Feasibility for hyperthermia was measured using G2-D5 Series Multi-mode

1500W Driver from Nanoscale Biomagnetics. A solution of 5 mg of NiCu nanoparticles dispersed in 1 ml of water was placed into the G2-D5 coil and an alternating magnetic field at different intensities and frequencies was applied. A fiber optic sensor was used to detect and record the induced temperature of the solution.

Chapter 3: Fe_3O_4 nanoparticles

3.1 Morphology and structure

Prior to measurements and characterization, the produced Fe_3O_4 nanoparticles have shown high magnetic properties since they were highly attracted to magnets. In order to confirm the formation of the required Fe_3O_4 pure phase, the sample was characterized using X-ray diffractometer as shown in Figure 9. The X-ray diffraction pattern of the sample confirmed the formation of Fe_3O_4 FCC structure. The obtained peaks have been labelled according to the JCPDS No. 98-005-0273. Moreover, more information regarding the crystalline size was obtained from Scherer formula [13] based on the dependence of the full width at half maximum on the crystallite size diameter as seen in Eq. (1).

$$D_{XRD} = \frac{0.93\lambda}{\Delta 2\theta \cos\theta} \quad (1)$$

where D_{XRD} is the average crystallite size of the particles, λ is the wavelength of the applied (Cu-K_α) radiation, $\Delta 2\theta$ is the full width of the diffraction peak at its half maximum, and θ is the Bragg angle (angle between the incident beam and the plane of the crystal). According to Eq. (1), the $\Delta 2\theta$ of each peak in Figure 9 yields an average size of 65, 43, and 55 nm for synthesis at 275, 350, and 320 °C respectively.

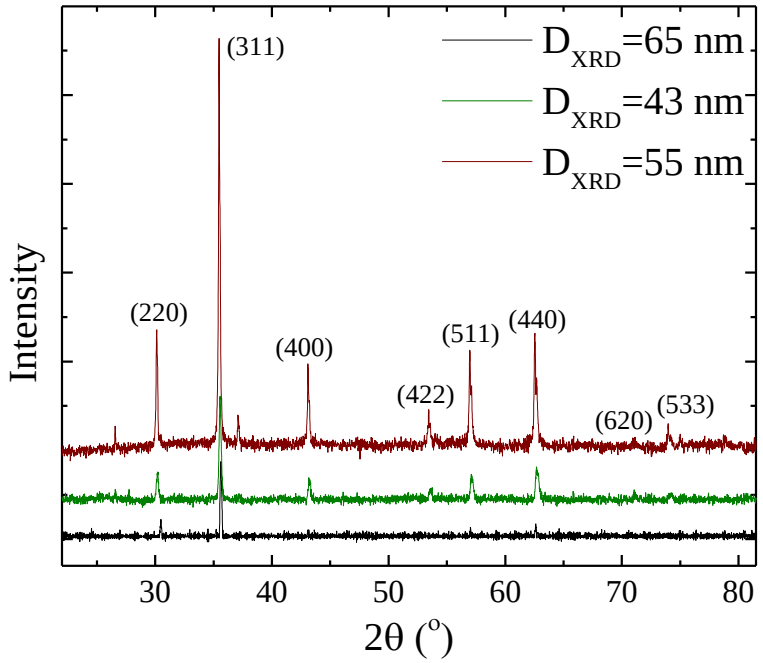

Figure 9 X-ray diffraction pattern of Fe_3O_4 nanoparticles

The morphology of the produced Fe_3O_4 nanoparticles was obtained using scanning electron microscopy (SEM) as shown in Figure 10 (left side) revealing cubic-like shape. The nanoparticles size distribution has been calculated and fitted by extreme fit as shown in Figure 10 (right side). The nanoparticles present a wide size distribution of 63±17, 128±19, and 90±28 nm respectively. Correspondence of particle size D_{SEM} and crystallite size D_{XRD} is shown in Table 1.

Table 1 Particle size D_{SEM} and crystallite size D_{XRD} of Fe_3O_4 nanoparticles.

D_{SEM}	D_{XRD}
(nm)	(nm)
63	65
128	43
90	55

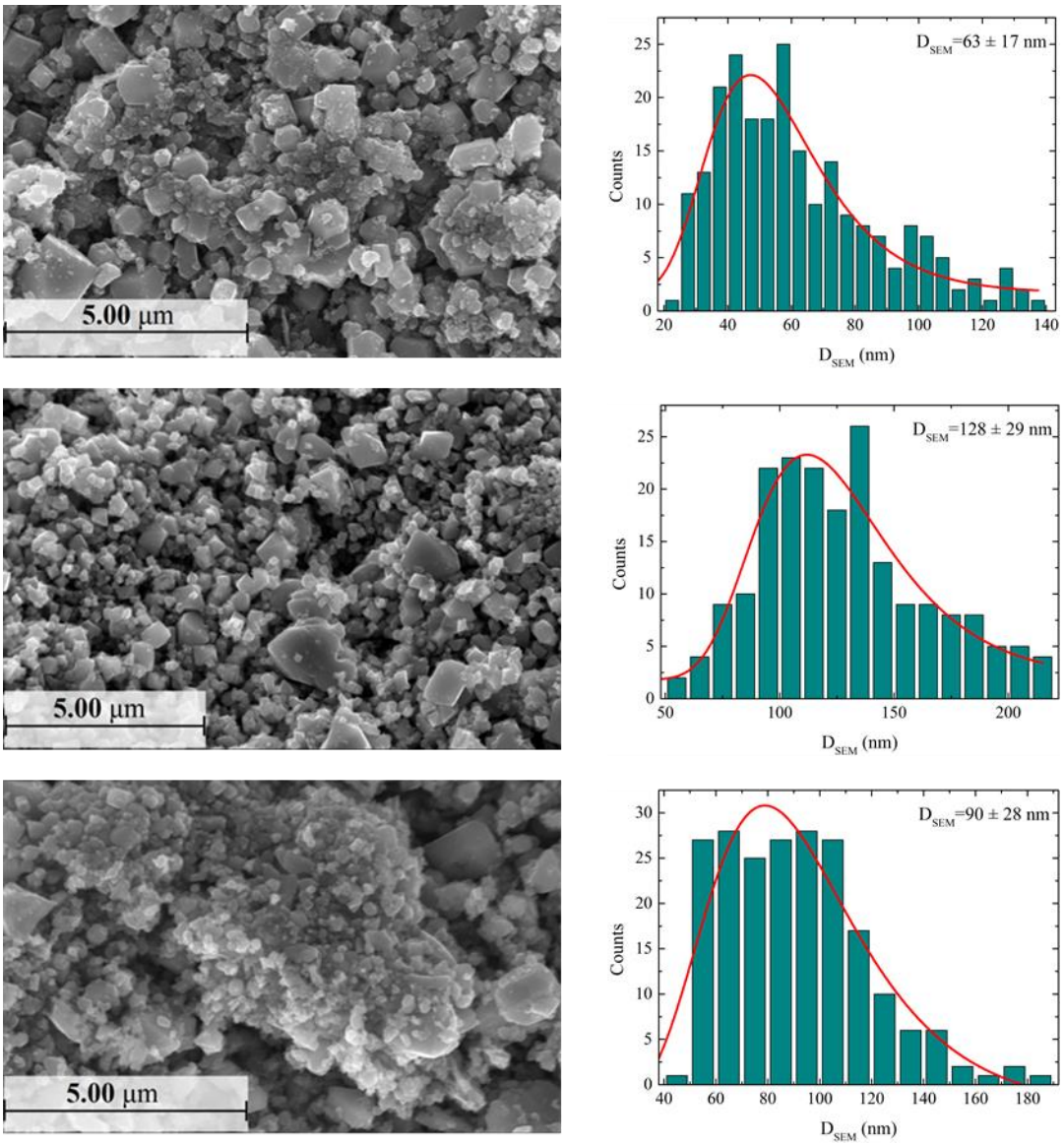

Figure 10 SEM images and size distribution for 63±30, 128±19, and 90±28 nm Fe_3O_4 nanoparticles

3.2 Magnetic properties

The study of the magnetic properties of Fe_3O_4 nanoparticles has been done by measuring the dependence of their magnetization on external magnetic field up to 3T at 300 K and on temperature at 100 Oe as shown in Figure 11 and Figure 12 respectively. The data obtained in

Figure 11 imply superparamagnetic-like behavior at 300 K as indicated by the closed hysteresis loop with high saturation magnetization of 108, 77, and 74 emu/g respectively. The Ms value for 63 nm nanoparticles is higher than the saturation magnetization value of their bulk candidate, confirming the possibility of enhancing magnetic properties at nanoscale. The value of remnant magnetization Mr is significantly small, as well as the coercivity is close to zero. All the magnetic measurement data including the particles size are listed in Table 1. Since the hysteresis loop is closed and the sample behaves like superparamagnetic (SPM), the magnetic domain size D_{mag} was estimated from the initial slope of MxH closed hysteresis loop using Eq. (2) [67]

$$D_{mag} = \left[\frac{18k_B T\frac{dM}{dH}}{\pi\rho M_S^2}\right]^{\frac{1}{3}} \quad (2)$$

where k_B is the Boltzmann constant, T is the temperature during the hysteresis cycle (300 K), dM/dH is the initial slope near zero field, ρ is the bulk density value of the sample (5.175 g/cm^3 for Fe_3O_4), and M_s is the saturation magnetization. D_{mag} yields 5.9 nm, where such small magnetic domain size confirms the observation of superparamagnetic (SPM) behavior.

In addition, the magnetization dependence on the temperature at constant field of 100 Oe has been measured to explore the blocking temperature T_B that distinguishes between the superparamagnetic and the ferromagnetic behavior (Figure 12). To be specific, the sample was cooled down to 50 K in zero magnetic field then heated up to 400 K under 100 Oe while recording the magnetization change versus time as zero field cooling curve (ZFC). Then the sample was cooled down to 50 K in presence of 100 Oe while magnetization dependence on temperature as field cooling curve (FC) was recorded. The maxima of the ZFC curve presents the blocking temperature (T_B) to be 320, 235, and 192 K respectively as listed as well in Table 2.

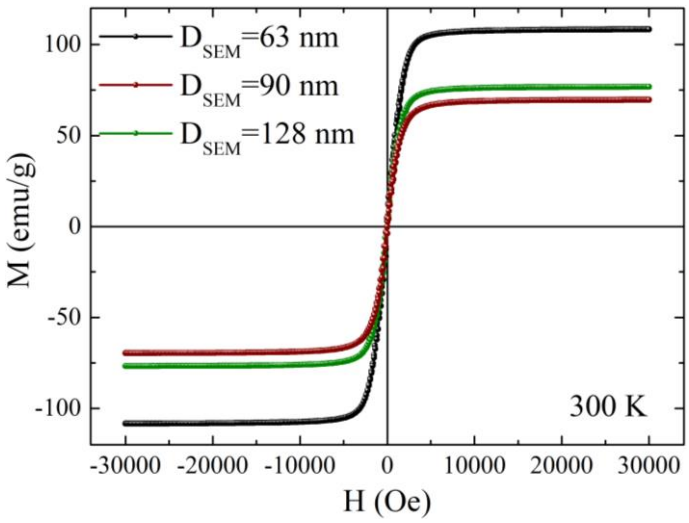

Figure 11 Hysteresis loops of Fe_3O_4 nanoparticles at room temperature and magnetic field up to 3T

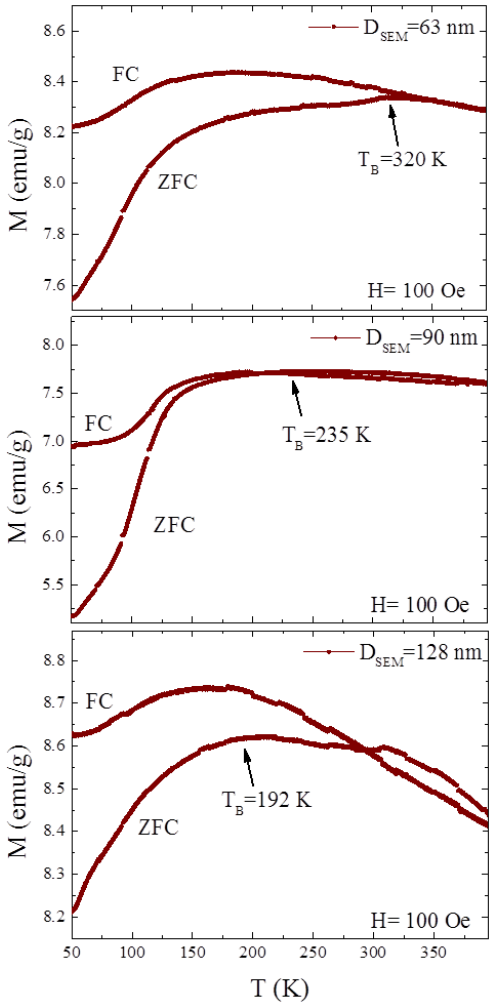

Figure 12 ZFC-FC curves of Fe_3O_4 nanoparticles at H =100 Oe

Table 2 Magnetic parameters of Fe_3O_4 synthesized at different temperatures and pressures

Fe_3O_4 samples	T	P	H_c	M_s	M_r	T_B	D_{mag}	D_{XRD}	D_{SEM}
	(°C)	(bar)	(Oe)	(emu/g)	(emu/g)	(K)	(nm)	(nm)	(nm)
	275	114	14	108	1.16	320	5.9	65	63 ± 17
	320	109	117	74	6.26	235	7.68	55	90 ± 28
	350	50	70	77	3.45	192	7.7	43	128 ± 19

3.3 Feasibility for hyperthermia measurement

In order to use the Fe_3O_4 nanocubes for medical application such as cancer treatment, their feasibility for hyperthermia has been measured. Here, the particles were dispersed in 1 ml distilled water then placed in small vial to be located in water cooled-coil connected to AC generator where magnetic field strengths and frequencies are applied. The effectiveness of the heat generation to the solution is determined by specific absorption rate (SAR). SAR is the rate at which mass absorbs electromagnetic energy when it is exposed to a magnetic field. It is given by Eq. (3) [68]

$$SAR = \frac{C_p}{m_{act}}\left(\frac{dT}{dt}\right)_{t=0} \quad (3)$$

where C_p is the water specific heat (4.18 $J \cdot g^{-1} \cdot K^{-1}$), m_{act} is the mass of the sample over the total mass (sample mass + 1 ml of distilled water) and $(dT/dt)_{t=0}$ is the initial slope of temperature-time data plotted in Figure 13 for 63 nm nanoparticles. Figure 14 shows the change in temperature on applied AC magnetic fields H at different frequencies *f (*144-304 kHz) for 63 nm nanoparticles. Figure 15 displays the SAR dependence on applied magnetic field (H=400 Oe) at different frequency range from 144-304 kHz. The figure shows that SAR values are proportional

to the applied magnetic field. Figure 16 shows SAR dependence on different applied AC magnetic fields H at *f*=304 kHz. The plots were fitted polynomial revealing that SAR is proportional to H^2.

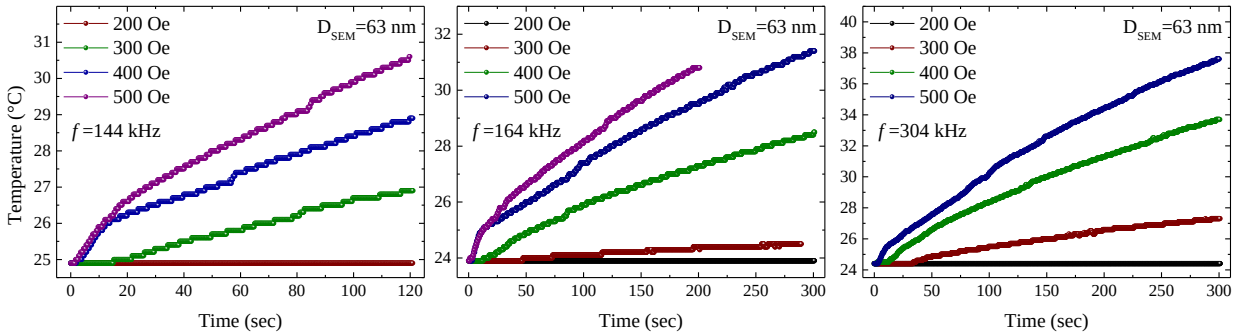

Figure 13 Temperature vs Time at different AC magnetic fields H and frequencies *f* for 63 nm particles

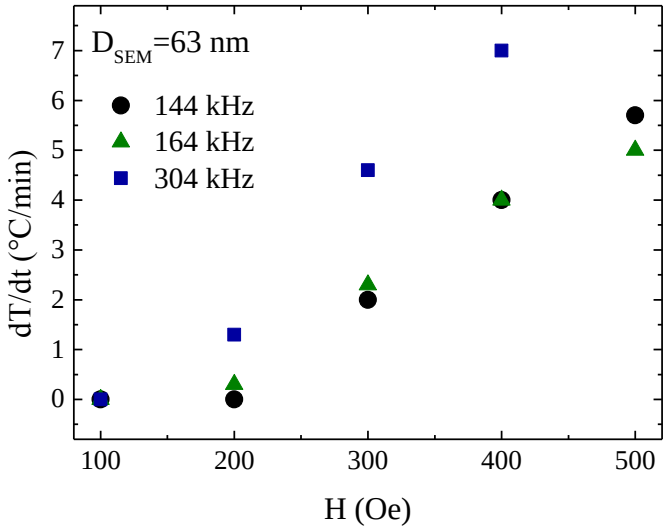

Figure 14 Change in temperature at different AC magnetic fields H and frequencies *f* for 63 nm particles

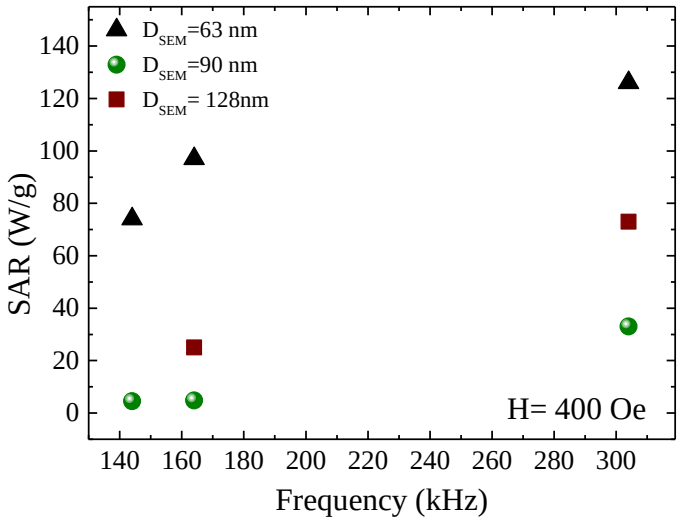

Figure 15 SAR dependence on applied AC magnetic field H=400 Oe at different frequencies *f*

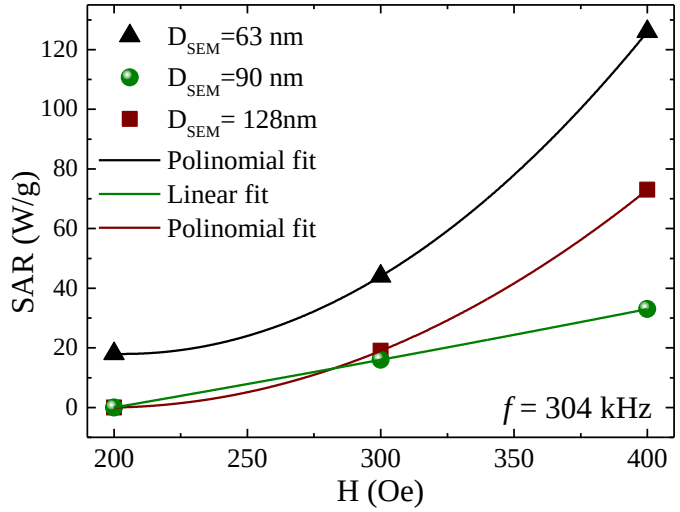

Figure 16 SAR dependence on different applied AC magnetic fields H at *f*=304 kHz

3.4 Discussion

The superparamagnetic Fe_3O_4 nanoparticles have been successfully prepared using supercritical condition of ethanol. In this method, iron precursor mixed with proper solvent and heated up to supercritical conditions of the solvent at high temperature and pressure where the precursor

decomposes to form stable pure phase of Fe_3O_4 nanoparticles. The nucleation of the particles occurred atom by atom at high temperature and pressure conditions producing homogeneous phase structure as well as well-defined cubic shape. XRD peaks confirmed the formation of Fe_3O_4 face centered cubic phase structure with average nanocrystalline sizes of 65, 55, and 43 nm. The SEM images of the sample revealed the formation of cubic-like shape with average particles size of 63, 90, and 128 nm in good agreement with the crystalline size calculated from XRD by Scherer equation. From the magnetic measurements, the formed particles yield superparamagnetic-like behavior in which the magnetic moments are randomly oriented by removing the applied magnetic field leading to closed hysteresis loop or zero H_C. This has been confirmed from the blocking temperature measurement using MxT curve. Such findings confirmed that the particles have superparamagnetic-like behavior at the therapeutic temperature range for hyperthermia therapy (42-47^oC), predicting significant heating power dissipated from the nanoparticles under applied external alternating magnetic field. As listed in Table 2, the data revealed higher magnetic properties in comparison to the previously published work [16-18]. The feasibility of those particles for hyperthermia has been examined to reveal that the increase of the applied magnetic field and frequency yields an increasing in the SAR values. Therefore, the Fe_3O_4 magnetic nanoparticles dispersed in water are exhibiting significant heating power, which make them feasible for hyperthermia treatment of cancer.

Chapter 4: Ni_xCu_{4-x} nanoparticles

4.1 Morphology and structure

Figure 17 shows the X-ray diffraction patterns of the six samples under study. Two different phases of Ni_xCu_{4-x} were found: $Ni_{0.2}Cu_{3.8}$ (Ref. JCPDS 98-062-8549) and $Ni_{3.68}Cu_{0.32}$ (Ref. JCPDS 98-062-8545). The area under the patterns' peaks reveal an average composition rate of 57% - 43% for Ni_xCu_{4-x} (x=0.2, 3.68). The crystallite size was found using Scherrer equation.

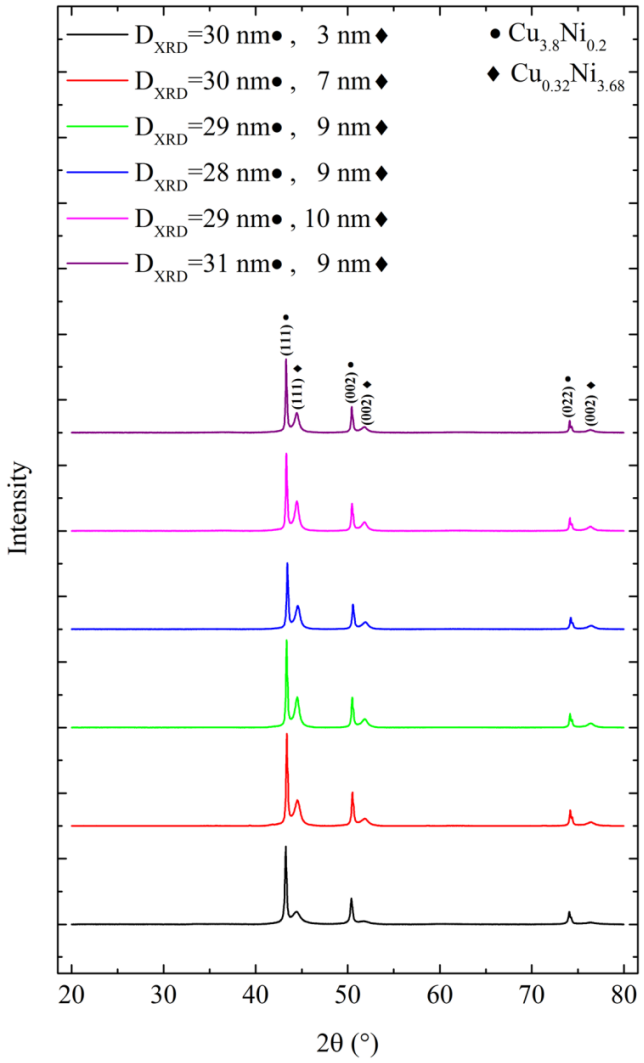

Figure 17 XRD pattern and crystallite size of NixCu4-x nanoparticles annealed at 300 °C for: a) 0 hr, b) 1 hr, c) 2 hr, d) 3 hr, e) 6 hr, and f) 10 hr

Scanning electron microscopy and transmission electron microscopy were used to study the morphology of the nanoparticles. Figure 18 shows SEM images and size distribution of Ni_xCu_{4-x} nanoparticles. It can be observed in SEM images that the samples present homogeneity in size distribution.

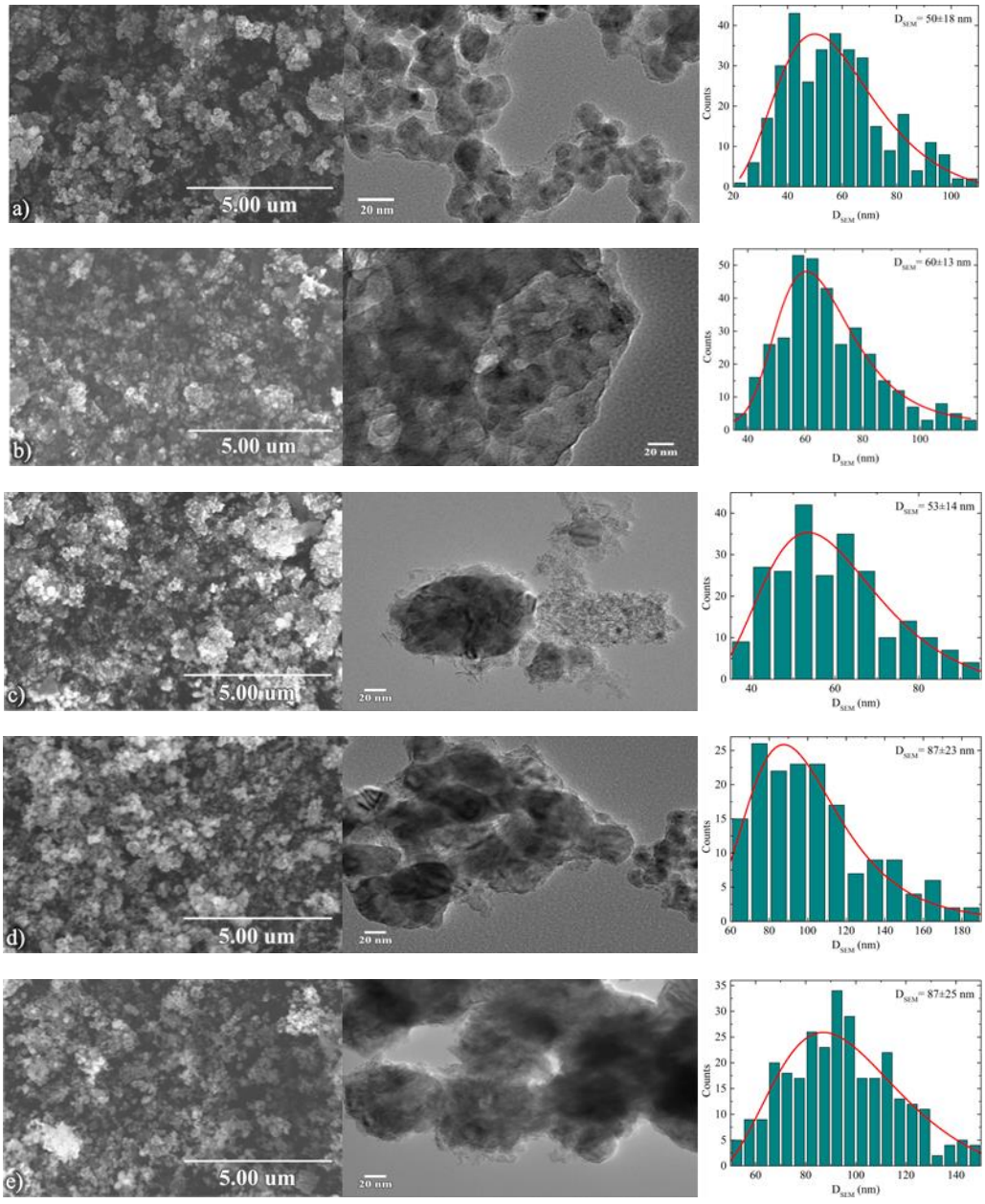

Figure 18 SEM, TEM, and size distribution of NixCu4-x nanoparticles (measured from SEM images) annealed at 300 °C for: a) 0 hr, b) 1 hr, c) 2 hr, d) 3 hr, and e) 6 hr

4.2 Magnetic properties

The dependence of magnetization on external magnetic field up to 3T at 300 K is shown in Figure 19. The close hysteresis loops imply superparamagnetic-like behavior as the remnant magnetization is significantly low and coercivity is close to zero, but further characterization shows that the samples present a collaborative behavior being closed-loop SD-ferromagnetic (single domain)[11].

Figure 20 shows the ZFC-FC curves of the samples at 200 Oe. The blocking temperature of the samples is between 196 K and 260 K, which is significantly lower than room temperature. Notice that the samples with the highest saturation magnetization (Ms) have the lowest blocking temperature (T_B).

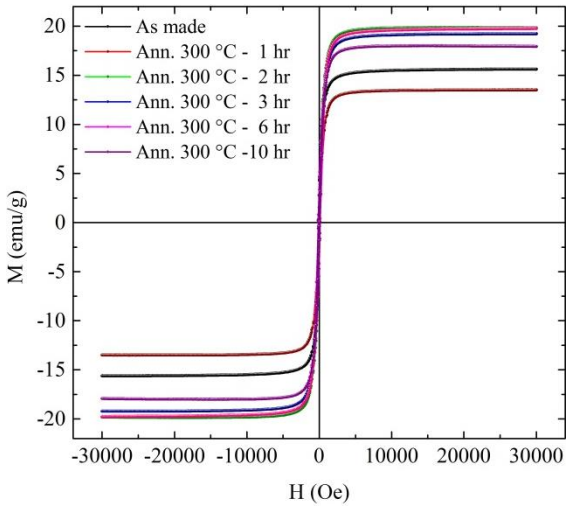

Figure 19 M-H curves of Ni_xCu_{4-x} nanoparticles

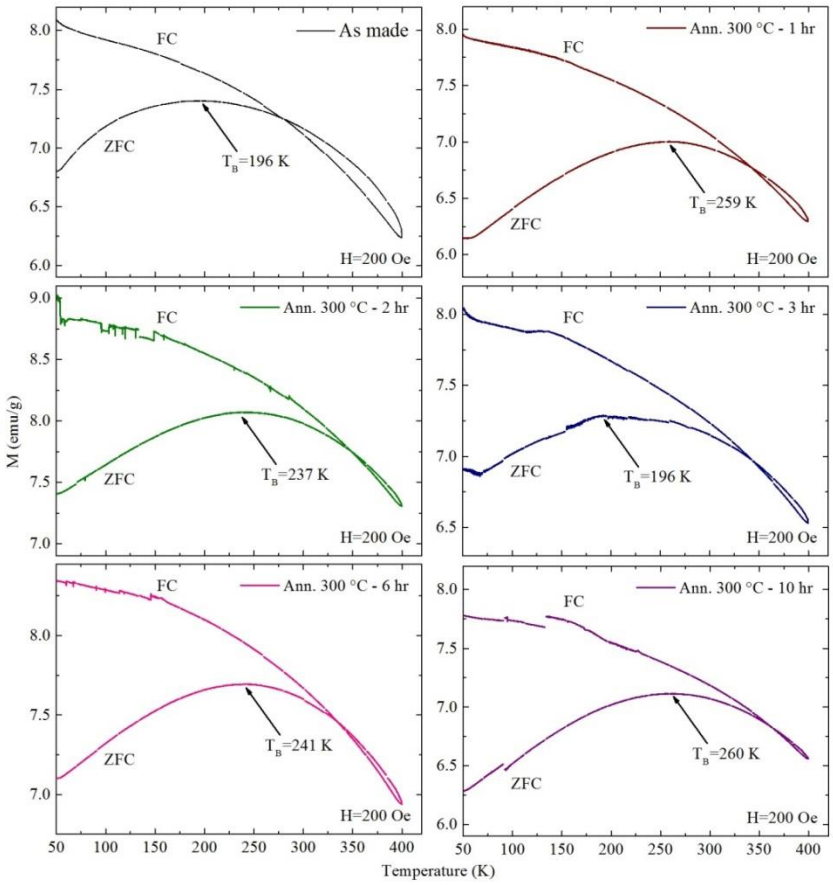

Figure 20 ZFC-FC curves of Ni_xCu_{4-x} nanoparticles

4.3 Feasibility for hyperthermia measurement

To test the Ni_xCu_{4-x} nanoparticles' feasibility for hyperthermia treatment of cancer, we dispersed each sample in water solutions with a 5 mg/ml concentration. The solutions were exposed to an alternating magnetic field at different amplitudes and frequencies, from 100 to 500 Oe and 144, 164, 304 kHz. Using a fiber-optic sensor, measurements of temperature versus exposure time (T-t) were recorded, as it is shown in Figures 21, 22, and 23 at 144, 164, and 304 kHz respectively. The figures only portray the magnetic field intensities at which heating occurred and the last one where there was no heating as reference. It can be observed that increasing the amplitude and frequency of the applied AC yields to higher temperatures due to the faster rotation of the

magnetic moments and the particles themselves. Figure 24 shows the change in temperature over time on applied AC magnetic fields H at different frequencies *f*. Figure 25 shows the SAR dependence of the samples on applied AC magnetic fields H at different frequencies *f*. It can be observed that the samples annealed for 2, 3, and 6 hours yield the highest SAR values when submitted to an alternating 400 Oe at 304 kHz magnetic field.

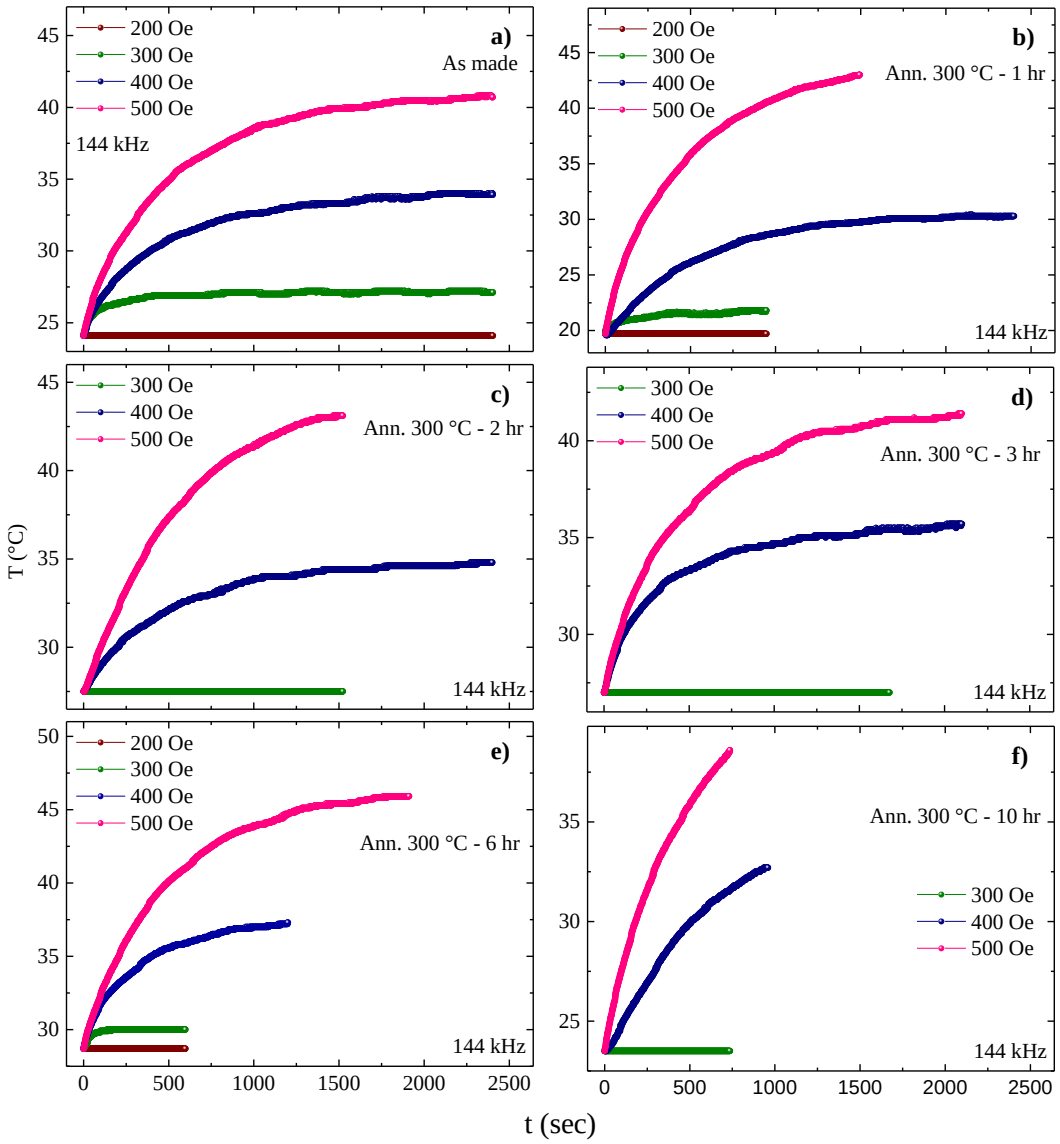

Figure 21 Temperature vs Time at different AC magnetic fields at 144 kHz for samples annealed at 300 °C for: a) 0 hr, b) 1 hr, c) 2 hr, d) 3 hr, e) 6 hr, and f) 10 hr

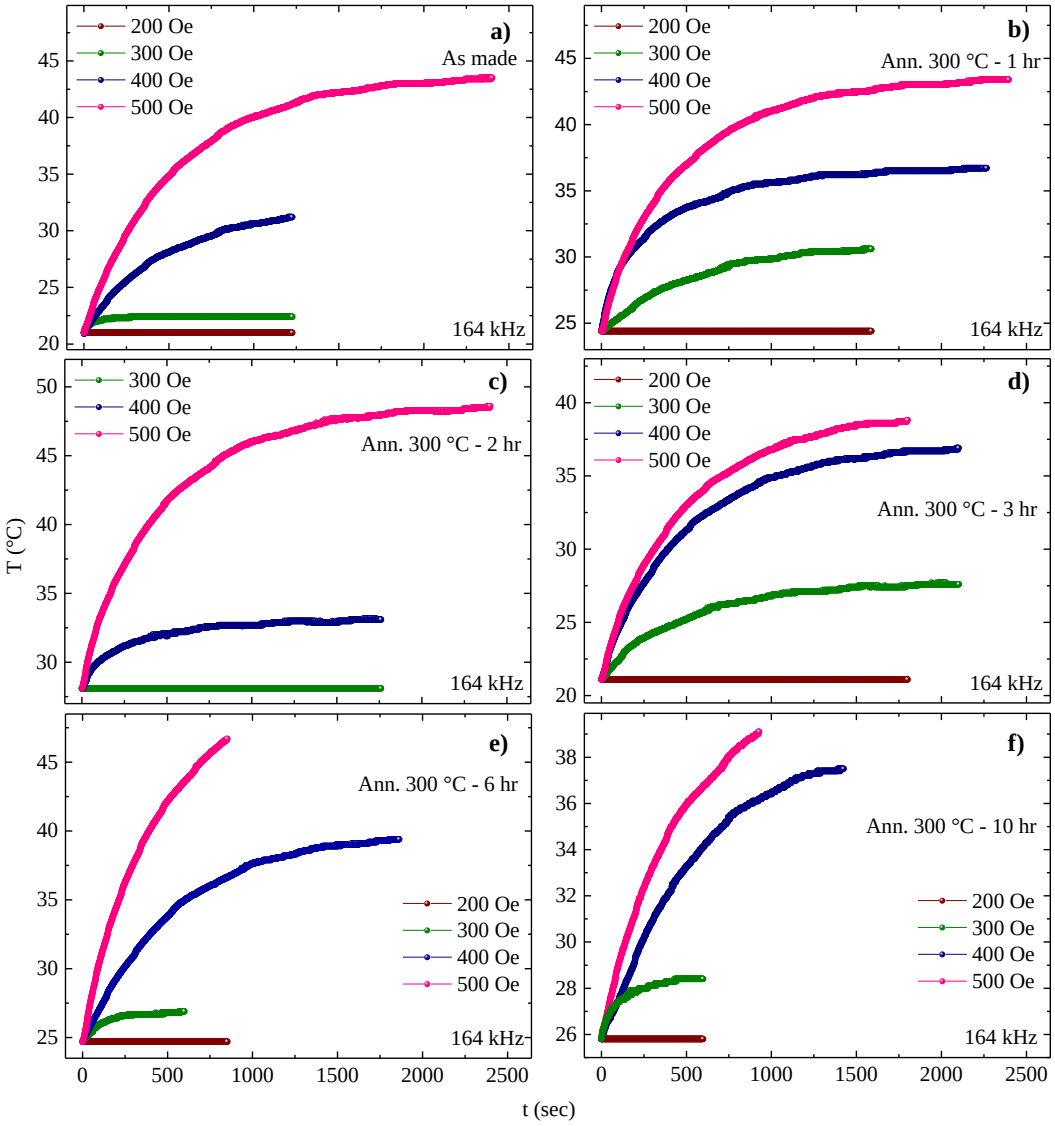

Figure 22 Temperature vs Time at different AC magnetic fields at 164 kHz for samples annealed at 300 °C for: a) 0 hr, b) 1 hr, c) 2 hr, d) 3 hr, e) 6 hr, and f) 10 hr

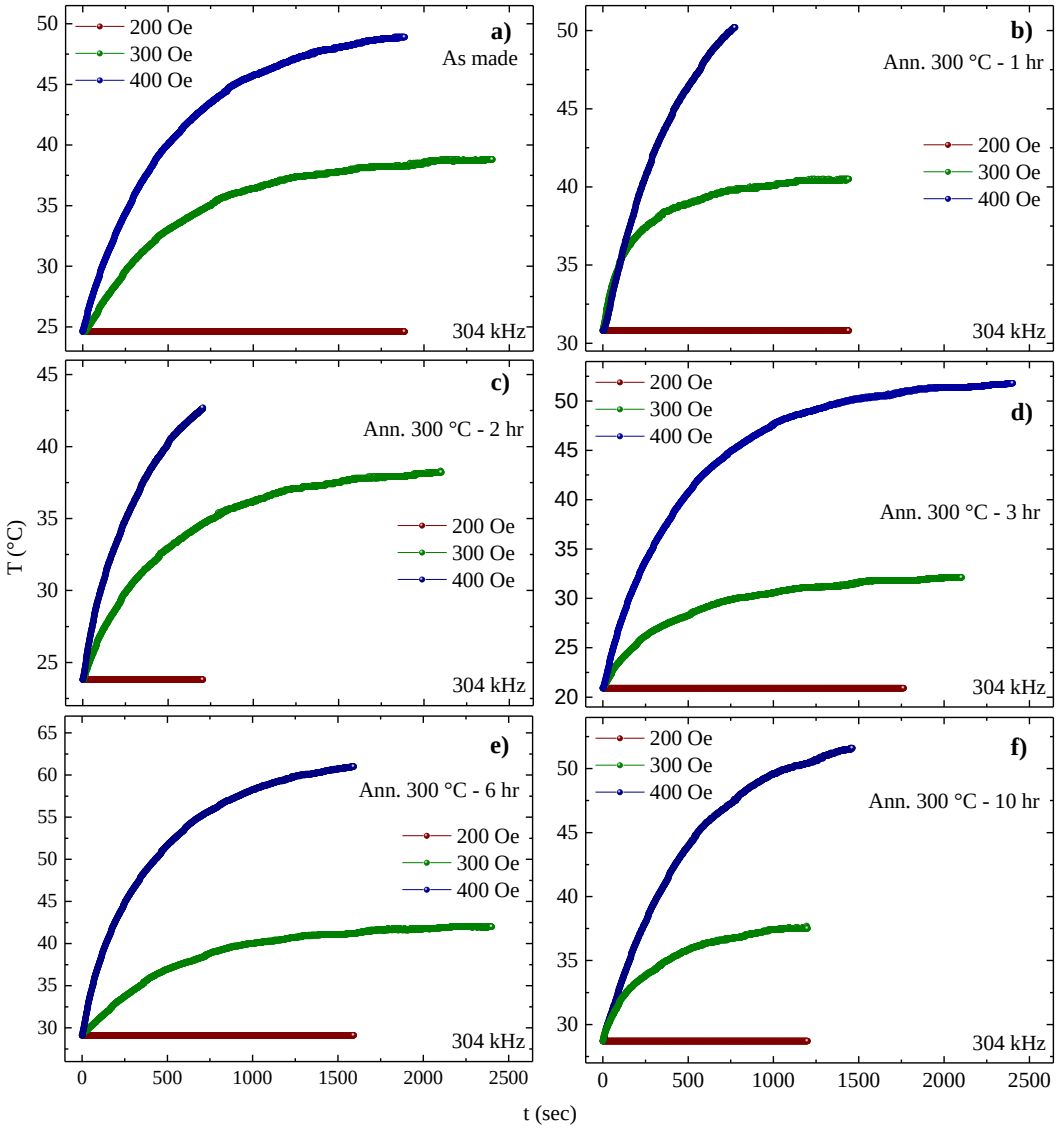

Figure 23 Temperature vs Time at different AC magnetic fields at 304 kHz for samples annealed at 300 °C for: a) 0 hr, b) 1 hr, c) 2 hr, d) 3 hr, e) 6 hr, and f) 10 hr

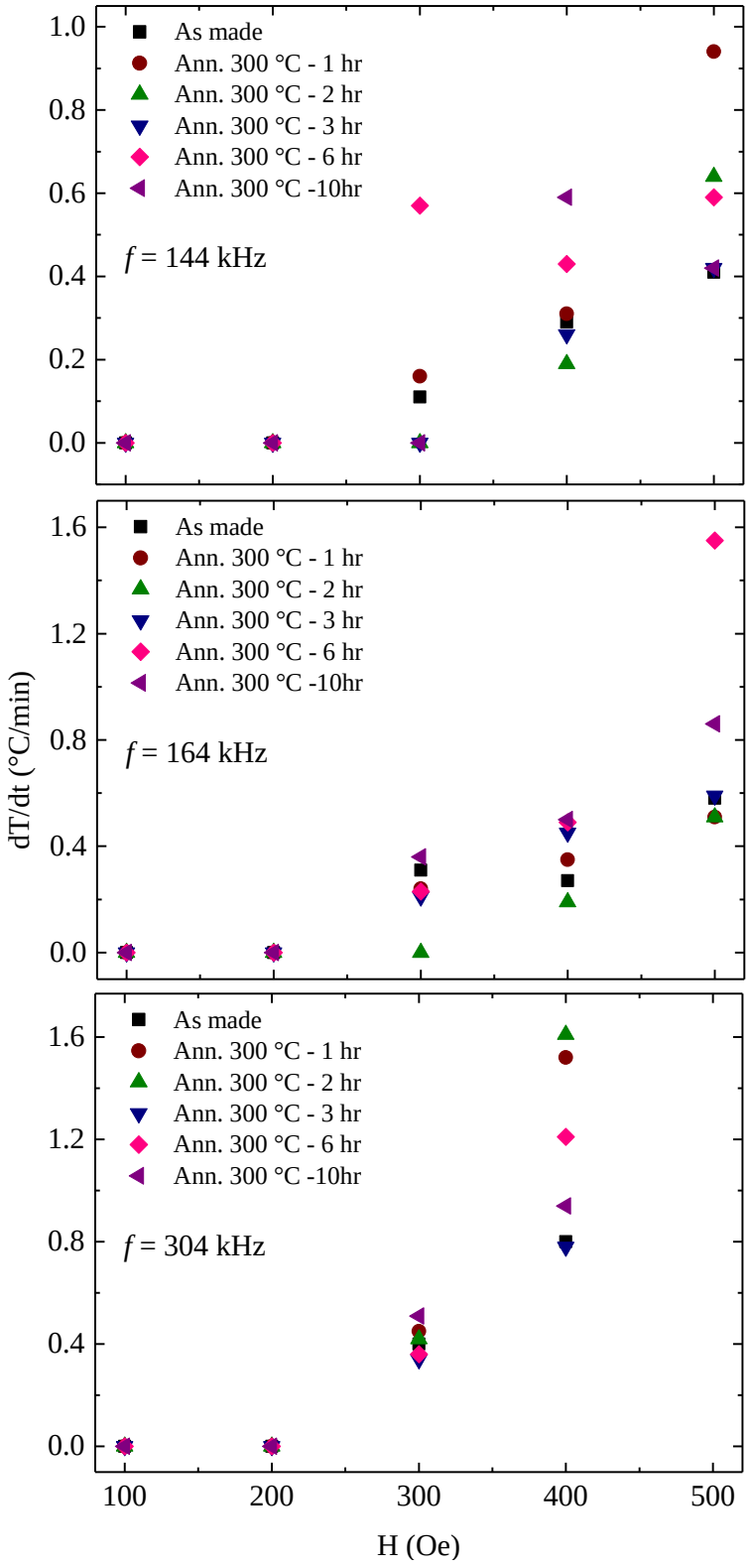

Figure 24 Change in temperature on applied AC magnetic fields H at different frequencies f for samples annealed at 300 °C for 0, 1, 2, 3, 6, and 10 hours

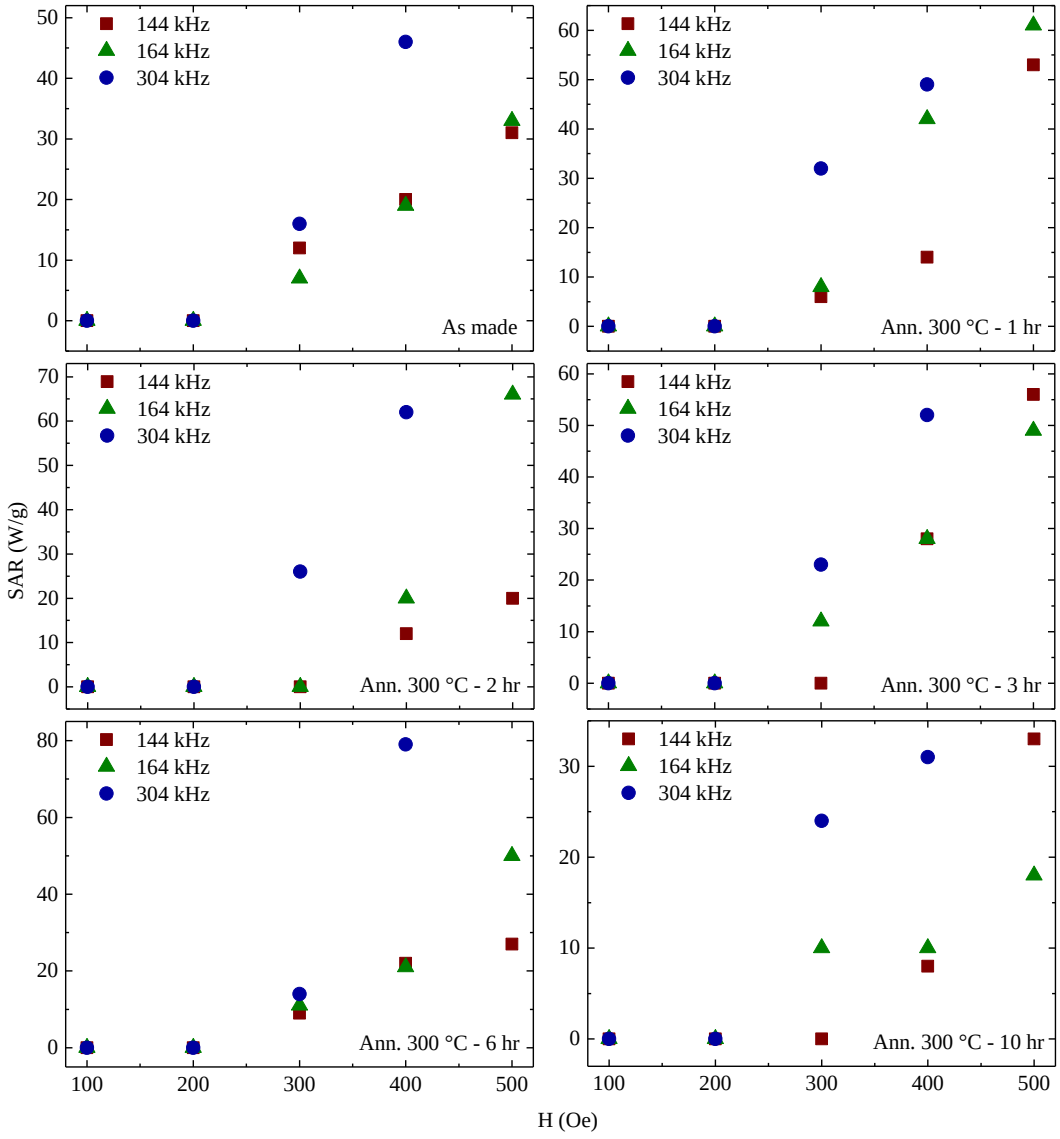

Figure 25 SAR dependence on applied AC magnetic fields H at different frequencies f for samples annealed at 300 °C for 0, 1, 2, 3, 6, and 10 hours, respectively

4.4 Discussion

Ni_xCu_{4-x} (x=0.2, 3.68) nanoparticles have been synthesized by reducing Ni and Cu from metal precursors using sol-gel route followed by annealing at 300^{o}C at different time intervals for controlled self-regulating magnetic hyperthermia application (SrMH). SEM, TEM, and XRD reveal spherical 50-87 nm nanoparticles (D_{SEM}) with FCC cubic structure for different

compositions of Ni_xCu_{4-x} in good agreement with the crystalline size calculated from XRD by Scherrer equation. Closed hysteresis loops indicate single domain (SD) ferromagnetic behavior in which the magnetic moments are randomly oriented by removing the applied magnetic field leading to closed hysteresis loop or zero H_C and with saturation magnetization (Ms) ranging from 13-20 emu/g at 300 K and Curie temperature (T_C) ranging from 42-45°C within the therapeutic temperature limit. The feasibility of hyperthermia has been performed under the therapeutic limits of AC magnetic field. Compared to the Fe_3O_4 nanoparticles' linear-like heating curves, Ni_xCu_{4-x} nanoparticles present temperature saturation at therapeutic range, which confirms the single domain ferromagnetic behavior and self-regulated magnetic hyperthermia. The samples exhibited heating rate and a significant dissipated heating power measured as specific absorption rate (SAR). Results reveal nanoparticles' feasibility for self-regulating hyperthermia.

Chapter 5: Conclusions

The study of magnetic nanoparticles for hyperthermia treatment has become a very significant research field for cancer therapy since it can revolutionize the way cancer patients are treated. Being able to provide a less invasive and nonaggressive option for treating cancer, compared to other kinds of treatments such as chemotherapy and radiotherapy, could help the patients undergo treatment in a shorter period of time without experiencing the known traumatic secondary effects cancer treatment has nowadays.

There are many parameters that need to be controlled when magnetic nanoparticles are prepared for this kind of studies to guarantee they will be safe for in vivo experiments and for further clinical trials.

In this work, superparamgnetic Fe_3O_4 nanoparticles dispersible in water have been synthesized at supercritical conditions of liquids. XRD and SEM measurements showed that the nanoparticles have Fe_3O_4 FCC structure with cubic-like shape of average size 63, 90, and 128 nm. The hysteresis loop shows superparamagnetic-like behavior at room temperature and high saturation magnetization, which makes the nanoparticles highly responsive to magnetic field and suitable for magnetic hyperthermia treatment. The particles exhibit blocking temperature at the therapeutic temperature range of hyperthermia therapy. Therefore, the SAR values were significant to show good potential of Fe_3O_4 nanoparticles to be perfect candidates for magnetic hyperthermia treatment for cancer.

Two phases of Ni_xCu_{4-x} nanoparticles (x=0.2, 3.68) have been successfully synthesized using sol-gel method followed by annealing at 300 °C for different during 0, 1, 2, 3, 6, and 10 hours. Morphology and crystal structure reveal spherical nanoparticles with cubic structure and average sizes measured from SEM images of 50-87 nm, and an average composition ratio of the

two Ni_xCu_{4-x} phases of 57% - 43% respectively. The magnetic properties showed superparamagnetic behavior for all the samples with an acceptable saturation magnetization at room temperature. The feasibility of hyperthermia was performed under the therapeutic limits of alternating magnetic field intensity and frequency. The samples exhibited heating rate and significant dissipated heating power, which reveals the potential of the Ni_xCu_{4-x} nanoparticles for hyperthermia treatment of cancer.

In future work, smaller particle sizes with narrower size distribution will be optimized, their feasibility for magnetic hyperthermia will be recorded, and in vitro/in vivo studies for tumor cells will be performed.

References

1. Cledon, M. and K.D. Hristovski, *The ongoing quest for understanding the novel environmental applications and implications of nanotechnology.* Science of The Total Environment, 2018. 618: p. 1088.
2. Singh, N.A., *Nanotechnology innovations, industrial applications and patents.* Environmental Chemistry Letters, 2017. 15(2): p. 185-191.
3. Arias, L.S., et al., *Iron Oxide Nanoparticles for Biomedical Applications: A Perspective on Synthesis, Drugs, Antimicrobial Activity, and Toxicity.* Antibiotics, 2018. 7(2): p. 46.
4. Wang, Z., et al., *Active targeting theranostic iron oxide nanoparticles for MRI and magnetic resonance-guided focused ultrasound ablation of lung cancer.* Biomaterials, 2017. 127: p. 25-35.
5. Qu, F., et al., *Programmed biomolecule delivery to enable and direct cell migration for connective tissue repair.* Nature Communications, 2017. 8(1): p. 1780.
6. Gazeau, A.K.A.S.A.E.J.K.T.C.W.F., *Iron Oxides: From Nature to Applications*. 2016. 590.
7. Lodhia, J., et al., *Development and use of iron oxide nanoparticles (Part 1): Synthesis of iron oxide nanoparticles for MRI.* Biomedical imaging and intervention journal, 2010. 6(2): p. e12.
8. Laurent, S., et al., *Magnetic fluid hyperthermia: Focus on superparamagnetic iron oxide nanoparticles.* Advances in Colloid and Interface Science, 2011. 166(1): p. 8-23.
9. Gupta, A.K. and M. Gupta, *Synthesis and surface engineering of iron oxide nanoparticles for biomedical applications.* Biomaterials, 2005. 26(18): p. 3995-4021.

10. Wu, W., Q. He, and C. Jiang, *Magnetic Iron Oxide Nanoparticles: Synthesis and Surface Functionalization Strategies.* Nanoscale Research Letters, 2008. 3(11): p. 397.

11. Boekelheide, Z., et al., *Gd5Si4 Micro- and Nano-Particles for Self-Regulated Magnetic Hyperthermia.* IEEE Transactions on Magnetics, 2017. 53(11): p. 1-4.

12. Stark, D.D., et al., *Superparamagnetic iron oxide: clinical application as a contrast agent for MR imaging of the liver.* Radiology, 1988. 168(2): p. 297-301.

13. Saallah, S.L., Wuled, *Nanoparticles Carrying Biological Molecules: Recent Advances and Applications*. Vol. 2018. 2018.

14. al., G.Y.e., *Nanomaterials Handbook*. 2006.

15. Lei Nia, e.a., *Decomposition of metal carbides as an elementary step of carbon nanotube synthesis.* Carbon 2009 47: p. 8.

16. Laurent, S., et al., *Magnetic Iron Oxide Nanoparticles: Synthesis, Stabilization, Vectorization, Physicochemical Characterizations, and Biological Applications.* Chemical Reviews, 2008. 108(6): p. 2064-2110.

17. Cuenya, B.R., *Synthesis and catalytic properties of metal nanoparticles: Size, shape, support, composition, and oxidation state effects.* Thin Solid Films, 2010. 518(12): p. 3127-3150.

18. Bhatia, S., *Nanoparticles Types, Classification, Characterization, Fabrication Methods and Drug Delivery Applications*, in *Natural Polymer Drug Delivery Systems: Nanoparticles, Plants, and Algae*, S. Bhatia, Editor. 2016, Springer International Publishing: Cham. p. 33-93.

19. Purcell, E.M., *Electricity and Magnetism*. 2nd ed. 1985, New York, NY: McGraw-Hill.

20. K., C.F., *Síntesis y Caracterización de Nanopartículas Magnéticas*, in *Centro de Investigación en Óptica*. 2013.

21. S., G.J., *Nanopartículas magnéticas para aplicaciones biomédicas*, in *Facultat de Farmacia*. 2012.

22. Alatorre, M.A.E.y.M., *Medición de Susceptibilidad Magnética X de Materiales*. 2005, CENAM: CENAM.

23. Kondo, J., *Resistance Minimum in Dilute Magnetic Alloys.* Progress of Theoretical Physics, 1964. 32(1): p. 37-49.

24. Cambridge, U.o. *Ferromagnetic Materials*. 2006; Available from: https://www.doitpoms.ac.uk/tlplib/ferromagnetic/index.php.

25. Eva Pavarini, E.K., Ulrich Schollwöck, *Emergent Phenomena in Correlated Matter*. Lecture Notes of the Autumn School Correlated Electrons 2013, ed. E.K. Eva Pavarini, Ulrich Schollwöck. Vol. 3. 2013, Jülich, Germany: Forschungszentrum Jülich Zentralbibliothek, Verlag Jülich.

26. Spalding, N.A., *Magnetic materials : fundamentals and device applications*. 2006: Cambridge University Press.

27. Bertotti, G., *Chapter 4 - Magnetic Work and Thermodynamics*, in *Hysteresis in Magnetism*, G. Bertotti, Editor. 1998, Academic Press: San Diego. p. 103-125.

28. Shtrikman, S. and D. Treves, *Internal Structure of Bloch Walls.* Journal of Applied Physics, 1960. 31(5): p. S147-S148.

29. Alex Hubert, R.S., *Magnetic Domains The Analysis of Magnetic Microstructures*. 1998: Springer, Berlin, Heidelberg.

30. Richard P. Feynman, R.B.L., Matthew Sands, *The Feynman Lectures on Physics*. Vol. II. 1963: California Institute of Technology, CA.

31. Bean, C.P. and J.D. Livingston, *Superparamagnetism.* Journal of Applied Physics, 1959. 30(4): p. S120-S129.

32. Kündig, W. and R. Steven Hargrove, *Electron hopping in magnetite.* Solid State Communications, 1969. 7(1): p. 223-227.

33. Franco, V., et al., *Relationship between coercivity and magnetic moment of superparamagnetic particles with dipolar interaction.* Physical Review B, 2005. 72(17): p. 174424.

34. Fish, G.E., *Soft magnetic materials.* Proceedings of the IEEE, 1990. 78(6): p. 947-972.

35. Coey, J.M.D., *Hard Magnetic Materials: A Perspective.* IEEE Transactions on Magnetics, 2011. 47(12): p. 4671-4681.

36. Johnson, J., *Hydraulic-Electric Analogies, Part 5: Current and Electrical Fields*. 2014, Hydraulics and Pneumatics.

37. Venäläinen, A., *Modification of bare and functionalized Au(111) surfaces and ferromagnetism of Au and Pd nanoclusters*, in *114 Physical sciences*. 2018, University of Helsinki: Helsinki.

38. Tang, S.C.N. and I.M.C. Lo, *Magnetic nanoparticles: Essential factors for sustainable environmental applications.* Water Research, 2013. 47(8): p. 2613-2632.

39. Liu, W.-T., *Nanoparticles and their biological and environmental applications.* Journal of Bioscience and Bioengineering, 2006. 102(1): p. 1-7.

40. Linh, P.H., et al., *Magnetic nanoparticles: study of magnetic heating and adsorption/desorption for biomedical and environmental applications.* International Journal of Nanotechnology, 2011. 8(3-5): p. 399-413.

41. Ngomsik, A.-F., et al., *Magnetic nano- and microparticles for metal removal and environmental applications: a review.* Comptes Rendus Chimie, 2005. 8(6): p. 963-970.

42. Li, L., et al., *Synthesis, Properties, and Environmental Applications of Nanoscale Iron-Based Materials: A Review.* Critical Reviews in Environmental Science and Technology, 2006. 36(5): p. 405-431.

43. Akbarzadeh, A., M. Samiei, and S. Davaran, *Magnetic nanoparticles: preparation, physical properties, and applications in biomedicine.* Nanoscale Research Letters, 2012. 7(1): p. 144.

44. Stark, W.J., et al., *Industrial applications of nanoparticles.* Chemical Society Reviews, 2015. 44(16): p. 5793-5805.

45. Vaghari, H., et al., *Application of magnetic nanoparticles in smart enzyme immobilization.* Biotechnology Letters, 2016. 38(2): p. 223-233.

46. Govan, J., et al., *Recent Advances in the Application of Magnetic Nanoparticles as a Support for Homogeneous Catalysts.* Nanomaterials, 2014. 4(2): p. 222-241.

47. Dobson, J., *Magnetic nanoparticles for drug delivery.* Drug Development Research, 2006. 67(1): p. 55-60.

48. Arruebo, M., et al., *Magnetic nanoparticles for drug delivery.* Nano Today, 2007. 2(3): p. 22-32.

49. Namdeo, M., et al., *Magnetic Nanoparticles for Drug Delivery Applications.* Journal of Nanoscience and Nanotechnology, 2008. 8(7): p. 3247-3271.

50. Yallapu, M.M., et al., *PEG-Functionalized Magnetic Nanoparticles for Drug Delivery and Magnetic Resonance Imaging Applications.* Pharmaceutical Research, 2010. 27(11): p. 2283-2295.

51. Corr, S.A., et al., *Linear Assemblies of Magnetic Nanoparticles as MRI Contrast Agents.* Journal of the American Chemical Society, 2008. 130(13): p. 4214-4215.

52. Vuong, Q.L., et al., *A Universal Scaling Law to Predict the Efficiency of Magnetic Nanoparticles as MRI T2-Contrast Agents.* Advanced Healthcare Materials, 2012. 1(4): p. 502-512.

53. Abakumov, M.A., et al., *VEGF-targeted magnetic nanoparticles for MRI visualization of brain tumor.* Nanomedicine: Nanotechnology, Biology and Medicine, 2015. 11(4): p. 825-833.

54. Amiri, H., et al., *Alzheimer's Disease: Pathophysiology and Applications of Magnetic Nanoparticles as MRI Theranostic Agents.* ACS Chemical Neuroscience, 2013. 4(11): p. 1417-1429.

55. Tse, B.W.-C., et al., *PSMA-targeting iron oxide magnetic nanoparticles enhance MRI of preclinical prostate cancer.* Nanomedicine, 2015. 10(3): p. 375-386.

56. Tseng, H., et al., *Localised heating of tumours utilising injectable magnetic nanoparticles for hyperthermia cancer therapy.* IET Nanobiotechnology, 2009. 3(2): p. 46-54.

57. Thiesen, B. and A. Jordan, *Clinical applications of magnetic nanoparticles for hyperthermia.* International Journal of Hyperthermia, 2008. 24(6): p. 467-474.

58. Grüttner, C., et al., *Synthesis and functionalisation of magnetic nanoparticles for hyperthermia applications.* International Journal of Hyperthermia, 2013. 29(8): p. 777-789.

59. Jordan, A., et al., *Magnetic fluid hyperthermia (MFH): Cancer treatment with AC magnetic field induced excitation of biocompatible superparamagnetic nanoparticles.* Journal of Magnetism and Magnetic Materials, 1999. 201(1): p. 413-419.

60. Bañobre-López, M., A. Teijeiro, and J. Rivas, *Magnetic nanoparticle-based hyperthermia for cancer treatment.* Reports of Practical Oncology & Radiotherapy, 2013. 18(6): p. 397-400.

61. Johannsen, M., et al., *Clinical hyperthermia of prostate cancer using magnetic nanoparticles: Presentation of a new interstitial technique.* International Journal of Hyperthermia, 2005. 21(7): p. 637-647.

62. Cassim, S.M., et al., *Development of novel magnetic nanoparticles for hyperthermia cancer therapy*. SPIE BiOS. Vol. 7901. 2011: SPIE.

63. Lahiri, B.B., T. Muthukumaran, and J. Philip, *Magnetic hyperthermia in phosphate coated iron oxide nanofluids.* Journal of Magnetism and Magnetic Materials, 2016. 407: p. 101-113.

64. Shete, P.B., et al., *Magnetic chitosan nanocomposite for hyperthermia therapy application: Preparation, characterization and in vitro experiments.* Applied Surface Science, 2014. 288: p. 149-157.

65. Fortin, J.-P., F. Gazeau, and C. Wilhelm, *Intracellular heating of living cells through Néel relaxation of magnetic nanoparticles.* European Biophysics Journal, 2008. 37(2): p. 223-228.

66. Weitschies, W., et al., *MOBILITY OF MAGNETIC PEG-NANOPARTICLES IN BLOOD, LIVER AND SPLEEN OF RATS.* 2019.

67. El-Gendy, A.A., et al., *Morphology, Structural Control, and Magnetic Properties of Carbon-Coated Nanoscaled NiRu Alloys.* The Journal of Physical Chemistry C, 2010. 114(24): p. 10745-10749.

68. El-Gendy, A.A., et al., *The synthesis of carbon coated Fe, Co and Ni nanoparticles and an examination of their magnetic properties.* Carbon, 2009. 47(12): p. 2821-2828.

Vita

Bianca Paola Meneses Brassea was born in Hermosillo, Sonora, Mexico. She studied her Bachelor of Science in Physics at University of Sonora in Hermosillo, Sonora. Bianca began the Master of Science in Physics program at The University of Texas at El Paso (UTEP) in Spring 2018 and worked as a Teaching Assistant during her graduate studies. She joined Dr. Ahmed A. El-Gendy's research group in his Nanomagnetics and Biomaterials Laboratory (Nanoland), focusing on the synthesis and characterization of magnetic nanoparticles for medical applications. During her Master's, Bianca was able to present her research work at national and international conferences, such as MMM-Intermag, APS March Meeting, CAM Conference, International Materials Research Congress, and MMM Conference. Most travels were funded by APS and UTEP's Physics Department, Graduate School, and College of Science. With the support of Dr. El-Gendy, Bianca has one accepted publication, two papers under review, one to be submitted soon,and two more under preparation. She is the Master's in Physics Students representative at UTEP's Graduate Student Assembly (GSA) and member of American Physical Society (APS), American Physical Society Topical Group on Magnetism and its Applications (APS GMAG), Institute of Electrical and Electronics Engineers (IEEE), and the Institute of Electrical and Electronics Engineers Magnetics Society. Bianca will now pursue her Doctoral degree in Environmental Science and Engineering at The University of Texas at El Paso.

Contact Information : <bmenesesbr@miners.utep.edu>